The Journal of Immunology

Size-Dependent Attenuation of TLR9 Signaling by Gold Nanoparticles in Macrophages

Chiau-Yuang Tsai, Shiou-Ling Lu, Chia-Wen Hu, Chen-Sheng Yeh, Gwo-Bin Lee and Huan-Yao Lei

J Immunol 2012; 188:68-76; Prepublished online 7 December 2011;
doi: 10.4049/jimmunol.1100344
http://www.jimmunol.org/content/188/1/68

The Journal of Immunology is published twice each month by
The American Association of Immunologists, Inc.,
1451 Rockville Pike, Suite 650, Rockville, MD 20852

Print ISSN: 0022-1767 Online ISSN: 1550-6606.

Size-Dependent Attenuation of TLR9 Signaling by Gold Nanoparticles in Macrophages

Chiau-Yuang Tsai,* Shiou-Ling Lu,† Chia-Wen Hu,† Chen-Sheng Yeh,‡ Gwo-Bin Lee,§ and Huan-Yao Lei*,¶

Gold nanoparticles (GNPs), which are generally thought to be bio-inert and non-cytotoxic, have become one of the most ideal nanomaterials for medical applications. Once engulfed by phagocytes, the immunological effects of GNPs are still of concern and require detailed investigation. Therefore, this study explored the immunological significance of GNPs on TLR-mediated innate immunity in murine macrophages. GNP causes specific inhibition of TLR9 (CpG oligodeoxynucleotides; CpG-ODNs) signal in macrophages. The impaired CpG-ODN–induced TNF-α production is GNP concentration- and size-dependent in murine Raw264.7 cells: a GNP of 4 nm in size is more potent than a GNP of 11, 19, 35, or 45 nm in size. Consistent with cytokine inhibition, the CpG-ODN–induced phosphorylation of NF-κB and JNK as well as NF-κB activation are suppressed by GNPs. GNPs accumulate in lysosomes after phagocytosis and also increase TLR9-associated lysosomal cathepsin expression and activities, but this is irrelevant to TLR9 inhibition by GNPs in our studies. In addition, GNPs affected TLR9 translocation in response to CpG-ODNs and to phagosomes. Further exploring how GNPs inhibited TLR9 function, we found that GNPs could bind to high-mobility group box-1 (which is involved in the regulation of TLR9 signaling) inside the lysosomes. The current studies demonstrate that size-dependent inhibition of TLR9 function by GNP may be attributed to its binding to high-mobility group box-1. ***The Journal of Immunology*****, 2012, 188: 68–76.**

Macrophages are professional phagocytic cells that are resident in lymphoid and nonlymphoid tissues and play an important role in the body's defenses (1). Macrophages express a broad range of pathogen recognition receptors (PRRs) to recognize and internalize microorganisms, induce cytokine production, process Ag, then present Ag to T cells, and consequently induce adaptive immunity (2–4). TLRs are one of the most important PRRs to recognize distinct microbial components and directly activate APCs (2–4). Eleven TLRs have been identified in humans and 13 in mice and can be divided into two kinds: TLR1, TLR2, TLR4, TLR5, TLR6, and TLR11, which are expressed on the cell surface to sense various foreign components from outside, such as TLR4 for LPS and TLR2 for lipoteichoic acid (LTA) (5); and TLR3, TLR7/8, TLR9, and TLR10, which are localized in endolysosomes and recognize internalized components from pathogens, including dsRNA for TLR3, single-stranded RNA for TLR7, and unmethylated CpG oligodeoxynucleotides (CpG-ODNs) for TLR9 (5).

Upon stimulation, TLRs require additional proteins to be activated by their respective ligands such as high-mobility group box-1 (HMGB-1), the nucleic acid sensor. Recently, HMGB-1 has been shown to be involved in the regulation of TLR3, TLR7, and TLR9 functions (6–8). The absence of HMGB-1 impairs the activation of TLR3, TLR7, and TLR9 in macrophages, but not TLR2 and TLR4 (6, 8). HMGB-1 is constitutively associated with TLR9 and accelerates the redistribution of TLR9 to early endosomes in response to CpG-ODNs (6).

Nanomaterials, because of their surface-enhanced optical properties and large surface area, hold promise for their applications in biotechnology and biomedicine as diagnostic and therapeutic agents (9, 10). Gold nanoparticles (GNPs), also known as colloidal gold, have been recommended for the treatment of various diseases since the Middle Ages, although the active mechanism still remains poorly understood (11). GNP has many advantageous properties such as chemical stability, a highly electron-dense core, ease of manipulation of size and shape, and ease of conjugation to drugs and biomolecules (12–16). These characteristics make it a good candidate for the design of protein blockers and drug carriers. Moreover, its unique surface plasmon resonance and non-ionizing radiation absorption features also allow it to be used in photothermal therapy (12) and radiotherapy (17). Although GNP is generally thought to be inert and non-cytotoxic, immunotoxicity is still a concern when applied in biomedical use (18–20).

It has been reported that nanomaterials are mainly recognized and phagocytosed by macrophages once in the circulation (21, 22). The cellular responses induced by nanoparticles are found to be size dependent (23–25). Therefore, understanding the biological consequences after ingestion of the nanomaterials in the body is of great importance, particularly in phagocytes that are related to

*Department of Microbiology and Immunology, College of Medicine, National Cheng Kung University, Tainan 70101, Taiwan; †Institute of Basic Medical Sciences, College of Medicine, National Cheng Kung University, Tainan 70101, Taiwan; ‡Department of Chemistry, National Cheng Kung University, Tainan 70101, Taiwan; §Department of Engineering Science, National Cheng Kung University, Tainan 70101, Taiwan; and ¶Center of Infectious Disease and Signaling Research, College of Medicine, National Cheng Kung University, Tainan 70101, Taiwan

Received for publication February 7, 2011. Accepted for publication October 21, 2011.

This work was supported by grants from the National Science Council (NSC98-2120-M-006-001) of Taiwan.

Address correspondence and reprint requests to Dr. Huan-Yao Lei, Center of Infectious Disease and Signaling Research and Department of Microbiology and Immunology, College of Medicine, National Cheng Kung University, 1 University Road, Tainan 70101, Taiwan. E-mail address: hylei@mail.ncku.edu.tw

The online version of this article contains supplemental material.

Abbreviations used in this article: CpG-ODN, CpG oligodeoxynucleotide; CTSB, cathepsin B; CTSK, cathepsin K; CTSL, cathepsin L; CTSS, cathepsin S; DIF H_2O, 18-MΩ-deionized, 0.22-μm-filtered water; F-GNP, fluorescein-PEG–tagged GNP; GNP, gold nanoparticle; HMGB-1, high-mobility group box-1; HNP, hollow nanoparticle; LTA, lipoteichoic acid; NIK, NF-κB–inducing kinase; poly I:C, polyinosinic-polycytidylic acid; PRR, pathogen recognition receptor; SHB, sucrose homogenization buffer; TEM, transmission electron microscopy.

immunological effects. In the current study, we used the murine Raw264.7 macrophage cell line to investigate the consequences of GNP internalization. We found that GNPs engulfed by macrophages inhibit proinflammatory cytokine production by CpG-ODNs in a size-dependent manner. The GNPs accumulated in lysosomes also affect TLR9 translocation in response to CpG as well as to phagosomes. GNPs can bind the general DNA sensor HMGB-1 in the lysosomal compartment, which may lead to attenuation of TLR9 function.

Materials and Methods

Materials and cell culture

LTA, imiquimod (R837), and polyinosinic-polycytidylic acid (poly I:C) were from InvivoGen (San Diego, CA); CpG oligonucleotides (5′-TCCATGACGTTCCTGACGTT-3′; CpG-ODN 2395) and fluorescently labeled CpG oligonucleotides (of the same sequence) were purchased from Invivogen and TIB Molbiol (Chino, CA), respectively; and LPS (*Escherichia coli* serotype 055:B5) was from Sigma-Aldrich (St. Louis, MO). Griess reagent was purchased from Sigma-Aldrich. The primary Abs used, including rabbit p-Ab anti–p-IκBα, IκBα, p–NF-κB, NF-κB, p-JNK, JNK, p-ERK1/2, ERK1/2, p-p38, and p38, were purchased from Cell Signaling Technology (Beverly, MA). Rabbit anti-TLR9, goat anti-EEA1, mouse anti-cathepsin K, and mouse anti–α-tubulin were from Santa Cruz Biotechnology (Santa Cruz, CA). Rabbit anti–HMGB-1, rat anti–LAMP-1, rabbit anti-cathepsin B, and goat anti-cathepsin L and S were from Abcam (Cambridge, U.K.), BD Biosciences Pharmingen (San Jose, CA), Bio-Vision (Mountain View, CA) and R&D Systems (Minneapolis, MN), respectively. Murine Raw264.7 cells were cultured in DMEM supplemented with 10% FBS, L-glutamine at 37°C in a humidified atmosphere under 5% CO_2. RAW-Blue cells that stably express an NF-κB and AP-1–inducible SEAP were provided by Dr. Kuo-Feng Hua, originally purchased from InvivoGen (26). The SEAP activities were measured using QUANTI-Blue (InvivoGen) SEAP detection medium. The SEAP levels were determined using a spectrophotometer at 630 nm.

Generation of mouse bone marrow-derived macrophage cells

C57BL/6 mice (female, 8–12 wk old) were purchased from the Laboratory Animal Center of National Cheng Kung University and maintained in the pathogen-free facility. The animals were raised and cared for according to the guidelines set up by the National Science Council (Taiwan, Republic of China). The mouse experiments were approved by the institutional animal care and use committee. Bone marrow-derived macrophage cells were obtained by flushing the bones of the hind leg of C57BL/6 mice with RPMI 1640 (Invitrogen, Carlsbad, CA). Cells were then cultured for 6 d in RPMI 1640 with 10% heat-inactivated FCS (Thermo Scientific HyClone, South Logan, UT), recombinant murine granulocyte/M-CSF (10 ng/ml final concentration; Peprotech, Rocky Hill, NJ) in 10-cm Petri dishes at a concentration of 0.5×10^6 cells/ml. Macrophage cells were used for experiments on day 6.

Synthesis of different sizes of GNPs and fluorescein-PEG–tagged GNP preparation

GNPs were prepared according to the method developed by Frens (27). All glassware used in these preparations was thoroughly cleaned in aqua regia (3 parts HCl and 1 part HNO_3), and all solutions were made using 18-MΩ-deionized, 0.22-μm-filtered water (DIF H_2O). Briefly, 1 ml 12.7 mM chloroauric acid (Sigma-Aldrich) was added to 54 ml DIF H_2O, and the solution was heated to boiling. Next, 940 μl, 670 μl, and 470 μl 38.8 mM trisodium citrate solution (Merck KGaA, Darmstadt, Germany) were added to the solution to synthesize 19-, 35-, and 45-nm GNPs, respectively. For 11-nm GNP, 4 ml 12.7 mM chloroauric acid was added to 49 ml DIF H_2O, and then 5 ml 38.8 mM trisodium citrate solution was added to the boiling solution. Four-nanometer GNP was prepared by borohydride reduction of the gold salt. Briefly, 1.968 ml 12.7 mM chloroauric acid was added to 96.432 ml DIF H_2O. The chloroauric acid solution was stood on ice for 10 min. Then, 1 ml 50 mM trisodium citrate solution was added to the solution for 1 min prior to reduction by adding 0.6 ml 0.5 M ice-cold sodium borohydride solution (Sigma-Aldrich). All GNPs were washed with DIF H_2O and further concentrated by centrifugation to remove impurities. For fluorescein-PEG–tagged GNP (F-GNP) preparation, 4-nm GNP was functionalized with S–PEG3000–NH_2 (Rapp Polymere GmbH, Tübingen, Germany) prior to conjugation with NHS–fluorescein (Thermo Fisher Scientific, Rockford, IL). The F-GNPs were further purified and concentrated by centrifugation. Transmission electron microscopy (TEM) assessment confirmed a good distribution. The fluorescent emission peak of F-GNPs was 521 nm by excitation at 495-nm light.

Microscopic observation

For observing the intracellular trafficking of GNPs, Raw264.7 cells (5×10^4) were seeded on glass coverslips in each well of 24-well plates and incubated with F-GNPs at 40 μg/ml at 37°C for 15, 30, 60 min or 24 h. At various time points postincubation, the cells were fixed with 4% paraformaldehyde, pH 7.4, at room temperature for 10 min, and then washed three times with PBS. Anti-EEA1 and anti–LAMP-1 primary Abs, followed by Alexa 594-labeled secondary Ab (Invitrogen), were used for early endosome and late endosome/lysosome staining. Prepared cells were mounted with mounting medium and photographed using Olympus FV1000 confocal microscopy, and the Workstation system was used for data analysis. Other fluorescent microscopy examinations including TLR9 immunofluorescent staining and CpG-ODN–FITC intracellular trafficking were similar to the above description. For TEM analysis, 4-nm GNP-treated Raw264.7 cells at 24 h were fixed with 4% glutaraldehyde and postfixed in 1% OsO_4. The cells were observed under a transmission electron microscope (Hitachi 7000, Tokyo, Japan).

Cytokines and nitrite measurement

All cytokines in conditioned medium were determined by using a commercial ELISA kit following the manufacturer's protocol (R&D Systems). The nitrite level was determined by modified Griess reagent (Sigma-Aldrich).

Western blotting analysis

The Raw264.7 cells were lysed in cell lysis buffer (Cell Signaling Technology), kept on ice for 30 min, and centrifuged at 12,000 rpm for 30 min. The supernatant was collected, and total protein concentration of the samples was measured by Bio-Rad Protein Assay (Bio-Rad Laboratories, Hercules, CA). Equal amounts (50 μg) of cell lysates were fractionated by 12% SDS-PAGE. Then, the proteins were transferred onto a polyvinyl difluoride membrane. After the overnight incubation with appropriate primary Ab, the membrane was stained with proper secondary HRP-conjugated Abs (Cell Signaling Technology) and visualized with ECL detection reagents (PerkinElmer Life Sciences, Boston, MA).

Quantitative RT-PCR

Total RNA was extracted from cells using TRI Reagent (Molecular Research Center, Cincinnati, OH). One microgram of total RNA was used as a template to make the first strand of cDNA using the Promega reverse transcriptase system (Promega, Madison, WI). Mouse TLR9 primers used for the PCR reaction have been reported by Edwards et al. (28), and the sequences used were as follows: forward, 5′-TTGGT CTGCA CCTCC AACAG T-3′; reverse, 5′-TGGGC CCATT GTGAT GAAC-3′. The housekeeping gene β-actin was used as a reference, and the sequences were as follows: forward, 5′-TCACC CACAC TGTGC CCATC TACGA-3′; reverse, 5′-CAGCG GAACC GCTCA TTGCC AATGG-3′. Quantitative RT-PCR was performed on cDNA aliquots by using a KAPA SYBR FAST qPCR Kit (Kapa Biosystems, Woburn, MA).

Phagosome isolation

Raw264.7 cells (2×10^6) were preincubated with or without 4-nm GNPs for 24 h and further incubated with ~2×10^7 2.8-μm BSA-conjugated magnetite beads (Dynabeads M-280 Tosylactivated; Invitrogen) for various durations. The conjugation of BSA on the magnetite beads was performed according to the manufacturer's protocol. After rigorous washing in PBS, Raw264.7 cells were scraped into 3-ml sucrose homogenization buffer (SHB: 0.25 M sucrose in 10 mM Tris-HCL, pH 7.4) and pelleted by centrifugation. Cells were resuspended in 1 ml SHB and disrupted by passing them through a 25-gauge needle. The cell breakage was monitored by light microscopy until ~90% cells were disrupted. The disrupted cells were processed to purify intact phagosomes by magnetic separation. For CpG-ODN stimulation, Raw264.7 cells were pulsed for 30 min with magnetic beads and then chased for 90 min in the presence or absence of CpG-ODNs (0.5 μM). After washing with Tris buffer (150 mM KCl in 10 mM Tris-HCl buffer, pH 7.4), phagosome pellets were resuspended in 40 μl Tris buffer supplemented with protease inhibitor mixture and 1% Triton X-100. Protein concentrations were normalized by the Micro BCA Protein Assay Kit (Thermo Fisher Scientific), and 5 μg of proteins was analyzed by Western blot.

Cathepsin L activity assay

Cathepsin L activity was determined by using a commercial InnoZyme Cathepsin L Activity Kit, Fluorogenic, following the manufacturer's protocol (Calbiochem, EMD Chemicals, Darmstadt, Germany).

Isolation of GNP-bound proteins from lysosomes

Raw264.7 cells (1×10^7) were treated with 10, 20, and 40 μg/ml 4-nm GNPs for 24 h. After washing in PBS, GNP-containing Raw264.7 cells were scraped into 3 ml SHB and pelleted by centrifugation (1200 rpm for 6 min). Cells were resuspended in 1 ml SHB and disrupted by passing them through a 25-gauge needle. The cell debris and nondisrupted cells were pelleted by centrifugation at 1200 rpm for 10 min. The supernatants were processed to purify crude GNP-containing lysosomes by centrifugation at 8000 rpm for 15 min. After washing in Tris buffer, the pellets were lysed with 200 μl lysis buffer, kept on ice for 30 min, and centrifuged at 10,000 rpm for 15 min. The GNP-containing pellets were washed three times with PBS using vigorous pipetting to remove excess lysosomal proteins, followed by incubation with 50 mM DTT. After 18 h at 4˚C with intermittent shaking, the solutions containing displaced proteins were separated from the GNPs by centrifugation of the GNP aggregates and were then further analyzed by silver staining and Western blot.

HMGB-1 and GNP in vitro binding assay

Raw264.7 cells (3×10^7) were permeabilized with 2 ml digitonin (50 μg/ml) in ice-cold 0.25 M sucrose–HEPES–buffered saline supplemented with protease inhibitor mixture for 30 min at 4˚C prior to centrifugation at 12,000 rpm for 30 min at 4˚C. The supernatants containing cytoplasmic proteins were collected and filtered with a 100-kDa Amicon Ultra-4 Centrifugal Filter Unit (Millipore, Billerica, MA) to remove any cell debris contaminants. The filtered cytoplasmic proteins were further concentrated by using a 10-kDa Amicon Ultra-4 Centrifugal Filter Unit and washed with 10 mM phosphate buffer (pH 7.2) to remove any detergent, sucrose, and salts. Finally, the cytoplasmic proteins were concentrated and preserved in phosphate buffer. The total protein concentration of the samples was measured by Bio-Rad Protein Assay. Cytoplasmic proteins (1.2 μg) containing HMGB-1 were incubated with different amounts of GNPs at 4˚C overnight. The GNP bound fraction (GNP-absorbed) was separated by centrifugation (14,000 rpm, 2 h, 4˚C). The GNP bound materials (GNP-eluted) were eluted by 50 mM DTT at 4˚C overnight. Then, both the absorbed fraction and the GNP-eluted fraction were run on Western blot with anti–HMGB-1 Ab.

Statistical analysis

Statistical significance was determined by unpaired t test: $*p < 0.05$, $**p < 0.01$, $***p < 0.001$.

Results

GNPs specifically inhibit the CpG-induced cytokines and NO in macrophages

We first investigated the effect of GNPs on TNF-α production upon stimulation with various TLR ligands in macrophages. It was found that the TNF-α production induced by LTA (TLR2), poly I:C (TLR3), or LPS (TLR4) was not affected by GNPs and was sometimes even enhanced. In contrast, the CpG-ODN (TLR9)-induced TNF-α production was significantly inhibited at both 0.1 μM and 1 μM doses, whereas the imiquimod (TLR7)-induced TNF-α production was inhibited at a low dose of 1 μM (Fig. 1*A*). The CpG-ODN–induced IL-6, IL-12p40, and nitrite production were also inhibited in GNP-treated Raw264.7 cells (Fig. 1*B*). In addition, GNPs also showed efficient inhibition of CpG-ODN–induced, but not LPS-induced, TNF-α and IL-6 in bone marrow-

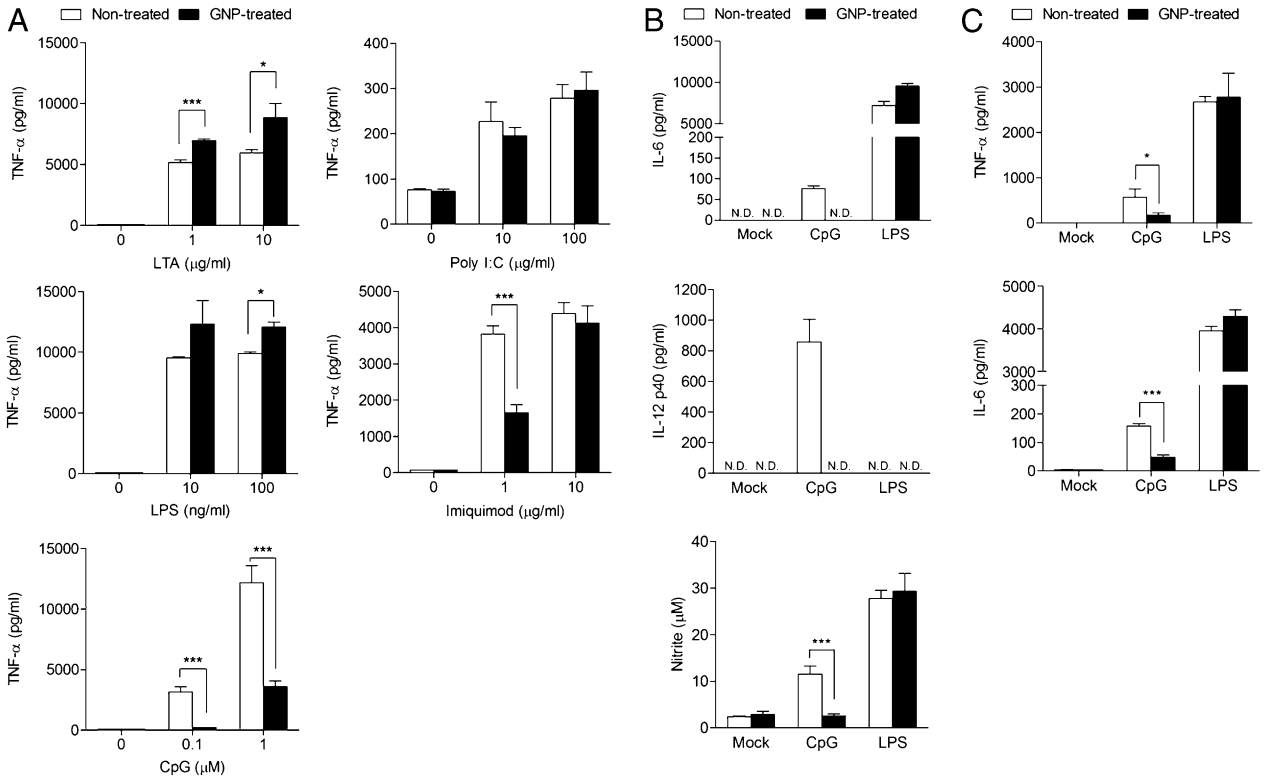

FIGURE 1. GNP attenuates the TLR signaling in macrophages. *A*, Four-nanometer GNP attenuates TLR9/7 agonist-induced TNF-α production in Raw264.7 cells. Raw264.7 cells pretreated with 40 μg/ml 4-nm GNPs for 24 h were then incubated with LTA (for TLR2), poly I:C (for TLR3), LPS (for TLR4), imiquimod (for TLR7), or CpG-ODNs (for TLR9) for 3 h. The TNF-α production was determined by ELISA. *B*, Four-nanometer GNP attenuates CpG-ODN–induced IL-6, IL-12p40, and nitrite production in Raw264.7 cells. Raw264.7 cells pretreated with 40 μg/ml 4-nm GNPs for 24 h were then incubated with LPS (10 ng/ml) or CpG-ODNs (0.1 μM) for 24 h. The IL-6 and IL-12p40 production was determined by ELISA. The nitrite production was determined by using modified Griess reagent. N.D., not detectable. *C*, Four-nanometer GNP attenuates CpG-ODN–induced TNF-α and IL-6 production in bone marrow-derived macrophages. Bone marrow-derived macrophages pretreated with 40 μg/ml 4-nm GNPs for 24 h were then incubated with LPS (10 ng/ml) or CpG-ODNs (1 μM) for 6 h. The TNF-α and IL-6 production was determined by ELISA. Error bars represent SDs from triplicate samples. The experiments were repeated at least three times.

derived macrophages (Fig. 1*C*). Furthermore, CpG-ODNs or LPS can enhance the cell surface expression of CD80, CD86, CD204, CD206, F4/80, and MHC class II molecules in Raw264.7 cells. However, only the CpG-ODN–induced surface expressions were inhibited by GNPs (Supplemental Fig. 1). Although TLR9 mRNA expression was slightly upregulated in the GNP-treated Raw264.7 cells (Supplemental Fig. 2*A*), the TLR9 functions were still inhibited by GNPs. Using the CpG-ODN–FITC to trace CpG-ODN intracellular traffic, GNPs did not inhibit the CpG-ODN uptake or its internalization in endosomes or lysosomes in Raw264.7 cells (Supplemental Fig. 2*C–E*). Based on the above data, we concluded that GNPs could inhibit the CpG-induced TLR9 functions in macrophages.

Size-dependent attenuation of TLR9 function by GNPs

We next examined whether the inhibitory effect of TLR9 signaling is dependent on GNP size. GNPs of different sizes ranging from ~4 to ~45 nm were prepared, and the TEM images confirmed their size distribution. The average diameter of GNPs was a) 3.8 ± 0.6 nm, b) 11.3 ± 1.3 nm, c) 19.2 ± 2.1 nm, d) 35.4 ± 5.6 nm, and e) 45.0 ± 4.3 nm, respectively (Fig. 2*A*, *a–e*). None of these sizes of GNP was cytotoxic to Raw264.7 cells at the high dose (40 μg/ml) tested (Fig. 2*A*, *f*). The inhibition of the CpG-ODN–induced TNF-α production was GNP size dependent, with the 4-nm size of GNP being the most potent (Fig. 2*B*). Although all sizes of GNP can be phagocytosed efficiently by Raw264.7 cells, the amount of uptake is greatest for the 35-nm size of GNP and least for the 4-nm size (Fig. 2*C*). However, when considering the number of GNPs taken up per cell, the cellular uptake of 4-nm GNP by Raw264.7 cells becomes the highest (Fig. 2*D*): the mean GNP numbers for sizes 4, 11, 19, 35, and 45 nm at a dose of 50 μg/ml are 8,291,959, 575,973, 103,368, 25,353, and 6,495, respectively. When calculating the total surface area of uptake of GNPs, 4-nm GNP also has the highest total surface area (Fig. 2*E*). Our data demonstrate that all sizes of GNPs could suppress CpG-ODN–induced TNF-α production in Raw264.7 cells. The most effective inhibition of the CpG-ODN–induced TNF-α production by the 4-nm GNP may be attributed to its greater cellular uptake and higher total surface area for modulation of TLR9 function.

GNP impairs CpG-ODN–induced activation of IκB/NF-κB and modulates the MAPK pathway

The TLR9 signaling cascade involves NF-κB–inducing kinase (NIK)–IKK–IκB and MAPK pathways, such as p38, JNK, and ERK (29, 30). To investigate which TLR9 signaling molecules were impaired by GNPs in Raw264.7 cells, the phosphorylation of NF-κB, IκB, JNK, p38, and ERK1/2 in CpG-ODN–stimulated Raw264.7 cells was compared with nontreated versus GNP-treated cells. In the NIK–IKK–IκB pathway, the kinetic phosphorylation of IκB-α showed a biphasic pattern with a first peak at 15 min and a second peak at 120 min after CpG-ODN treatment. However, the GNP pretreatment altered this pattern: the first peak of p–IκB-α at 15 min was increased, but the second peak at 120 min was decreased (Fig. 3*A*, *top panel*). The phosphorylation of NF-κB was also modulated accordingly. The p–NF-κB was decreased at 30 and 120 min after CpG-ODN stimulation in nontreated macrophages, but only p–NF-κB at 120 min was decreased in GNP-treated macrophages. The GNPs in lysosomes can therefore apparently modulate the IκB–NF-κB phosphorylation. Furthermore, the MAPK pathways were also altered in GNP-treated macrophages after CpG-ODN stimulation (Fig. 3*A*, *bottom panel*). The phosphorylation of JNK was inhibited in GNP-pretreated macrophages. In contrast, the phosphorylation of p38 was increased and sustained until 120 min after CpG-ODN

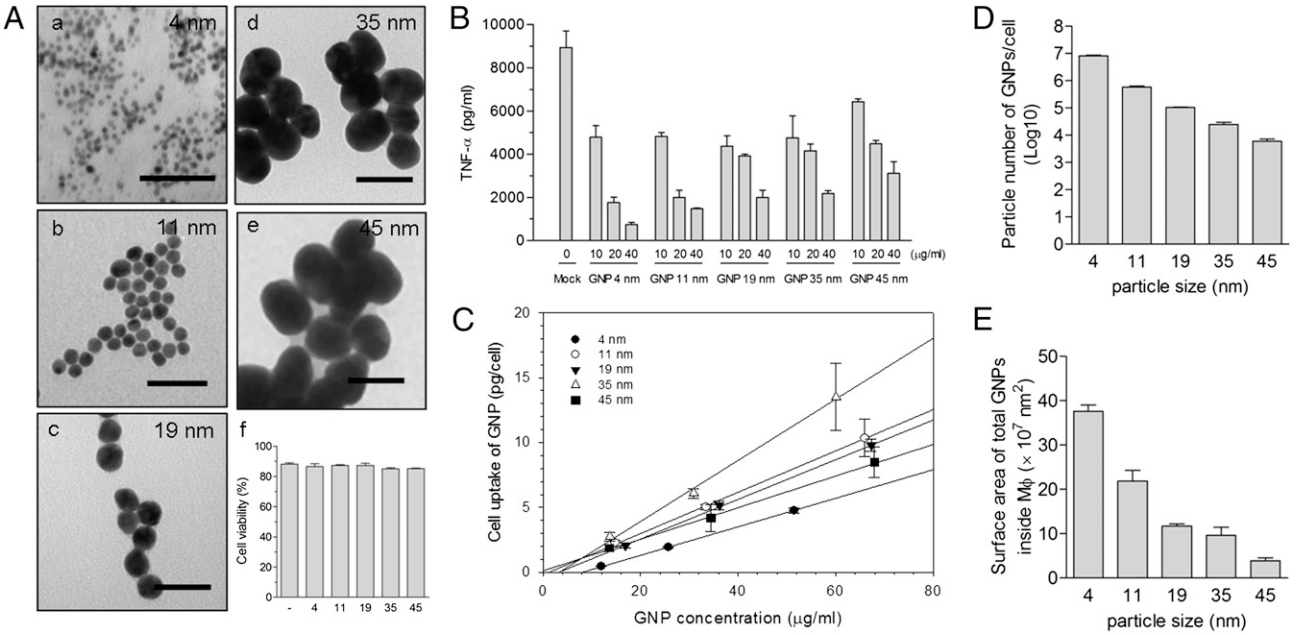

FIGURE 2. Size-dependent inhibition of CpG-ODN–induced TNF-α production by GNPs. *A*, The characteristics of GNPs with different sizes. *a–e*, TEM images of GNPs (~4, 11, 19, 35, and 45 nm; scale bars, 50 nm). *f*, No cytotoxicity of GNPs in Raw264.7 cells. Raw264.7 cells were treated with GNPs of different sizes at 40 μg/ml for 24 h. The GNP-treated Raw264.7 cells were stained with propidium iodide on flow cytometry to determine the cell viability. The cell viability (%) = 100% − propidium iodide-positive cell percentage. *B*, Size-dependent GNP inhibition of CpG-ODN–induced TNF-α production. GNP-treated Raw264.7 cells were stimulated with CpG-ODNs at 0.2 μM for 3 h. The TNF-α production was determined by ELISA. *C–E*, The cell uptake of GNPs in Raw264.7 cells. Raw264.7 cells were treated with various sizes and doses of GNPs for 24 h. The gold level in cells was determined by inductively coupled plasma atomic emission spectroscopy (*C*). The regression lines were determined by cellular uptake of GNPs correlated with GNP concentration. The R^2 values of each slope were close to 1.00. The number of GNPs taken up per cell for different sizes of GNPs at 50 μg/ml GNP treatment for 24 h (*D*). The total GNP surface area of different sizes of GNPs (*E*). Error bars represent SDs from triplicate samples.

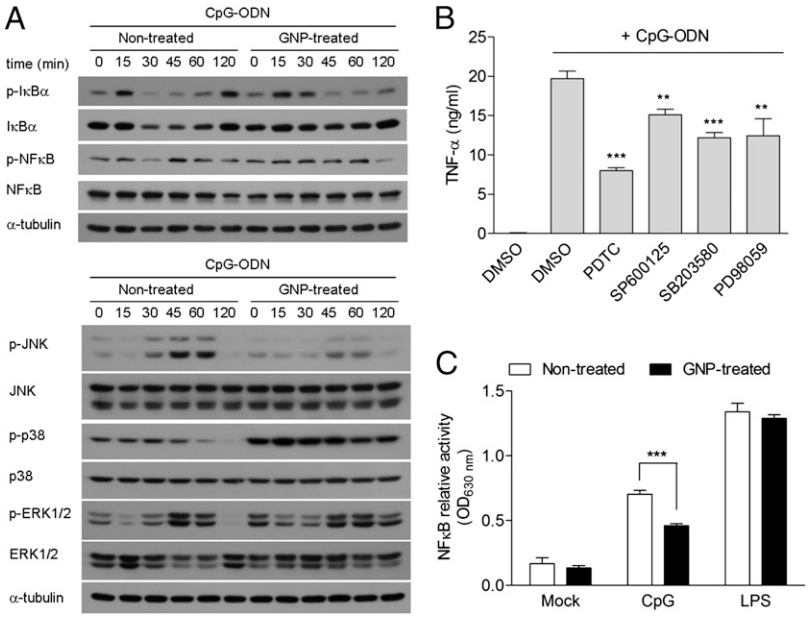

FIGURE 3. GNP impairs CpG-ODN–induced signaling pathway of IκB/NF-κB and MAPK pathway in Raw264.7 cells. *A*, Raw264.7 cells were pretreated with 40 μg/ml 4-nm GNPs for 24 h and then stimulated with 0.5 μM CpG-ODNs. At various times poststimulation, the lysates were analyzed by Western blot. *Top panel*, p–IκB-α, IκBα, p–NF-κB, and NF-κB expression. *Bottom panel*, p-JNK, JNK, p-p38, p38, p-ERK1/2, and ERK1/2. α-Tubulin was used as a loading control. *B*, Inhibition of CpG-ODN–induced TNF-α production. Raw264.7 cells were pretreated with pharmacological inhibitors of NF-κB (PDTC, 50 μM), JNK (SP600125, 10 μM), p38 (SB203580, 10 μM), and ERK (SB98059, 10 μM) for 45 min and then stimulated with CpG-ODNs (0.5 μM) for 3 h. The TNF-α was determined by ELISA. All inhibitors were diluted in DMSO. The samples treated with DMSO and stimulated with CpG-ODNs were used as a control group. The TNF-α production of all inhibitor treatments was compared with that of DMSO plus CpG-ODNs. *C*, CpG-ODN–induced NF-κB activation was impaired by GNPs. RAW-Blue cells were pretreated with 40 μg/ml 4-nm GNPs for 24 h and then stimulated with 0.1 μM CpG-ODNs or 10 ng/ml LPS for 24 h. Culture supernatant was collected to determine the secreted alkaline phosphatase as the NF-κB activity following the manufacturer's protocol. Error bars represent SDs from quadruplicate samples. The experiments were repeated at least two times.

stimulation in GNP-treated macrophages compared with that in nontreated macrophages. For ERK1/2 phosphorylation, there was still a higher level of p-ERK1/2 at 120 min in GNP-treated macrophages than that in the control. For the CpG-ODN–induced TNF-α production, these signal molecules were involved because inhibitors such as PDTC (for NF-κB), SP600125 (for JNK), PD98059 (for MEK1/2), or SB203580 (for p38) could inhibit the TNF-α production in Raw264.7 cells, and PDTC was the most potent (Fig. 3*B*). We further used a NF-κB reporter assay of secreted SEAP activity to evaluate the GNP effect. Fig. 3*C* shows that GNPs could attenuate CpG-ODN–stimulated, but not LPS-stimulated, NF-κB activation. Taken together, these findings suggest that GNP modulates CpG-ODN–induced NF-κB and MAPK pathways, and the NF-κB pathway seems to be the most important for the inhibition of TNF-α production.

GNPs accumulated in lysosomes enhance the expression and activities of cathepsin enzymes

To trace the localization of GNPs in macrophages, we prepared F-GNPs. Raw264.7 macrophage cells were incubated with F-GNPs for various times and observed under confocal microscopy. At 15 min postincubation, the F-GNP was first colocalized with early endosome marker EEA1-positive vesicles. At 30 min or thereafter, almost all of the F-GNP was colocalized with lysosome marker LAMP-1–positive vesicles (Fig. 4*A*). The electron microscopy observation also showed that the high electron density GNP is accumulated in lysosomes at 24 h (Fig. 4*B*). In addition, the accumulation of GNPs did not cause a significant lysosomal membrane permeability change in Raw264.7 cells (Supplemental Fig. 3). Recent reports have shown that specific inhibitors of cysteine proteases, including cathepsin K (CTSK), cathepsin L (CTSL), cathepsin S (CTSS), and cathepsin B (CTSB), can block the TLR9 signal transduction in dendritic cells and macrophages (31, 32). Gold compounds [Au (1)], including gold thiomalate (Myochrysin) and Auranofin, have been reported to inhibit these cathepsins in in vitro biochemical and cell-based assays (33, 34). Because GNP [Au (0)] preferentially binds to the sulfhydryl residues of proteins and influences their biological functions (14, 15), it is reasonable to presume that GNPs may have an inhibitory effect on cathepsin activities. Therefore, we determined the expression and activity of lysosomal proteases in GNP-treated macrophages. Expression of CTSL, CTSS, CTSB, and CTSK was upregulated in GNP-treated Raw264.7 cells 24 h later, and this enhancement occurred in a dose- and size-dependent manner (Fig. 4*C*). GNP of 4-nm size was the most potent in enhancing the cathepsin expression as shown by Western blot analysis. The enzyme activity of CTSL was also enhanced in a size-dependent manner, with the 4-nm size of GNP still observed to be the most potent (Fig. 4*D*). Thus, GNP accumulation in lysosomes enhances the expression and activities of cathepsin enzymes in macrophages. However, the elevation of cathepsins by GNPs may not be attributable to the attenuation of TLR9 signaling in our studies.

GNP affects the TLR9 translocation to sites of CpG and phagosomes

A previous study has shown that TLR9 could be recruited to endocytosed CpG DNA (35). TLR9 resides in the endoplasmic reticulum and will redistribute to endolysosomes (35, 36) and undergoes processing to generate functional receptors (37). To understand further how the GNPs accumulated in lysosomes affect CpG-ODN–induced TLR9 signaling, we incubated Raw264.7 cells with CpG-ODN–FITC and visualized TLR9 by immunofluorescence staining. Fig. 5*A* indicates that TLR9 translocates to sites of CpG-ODNs as early as 5 min after incubation in non-

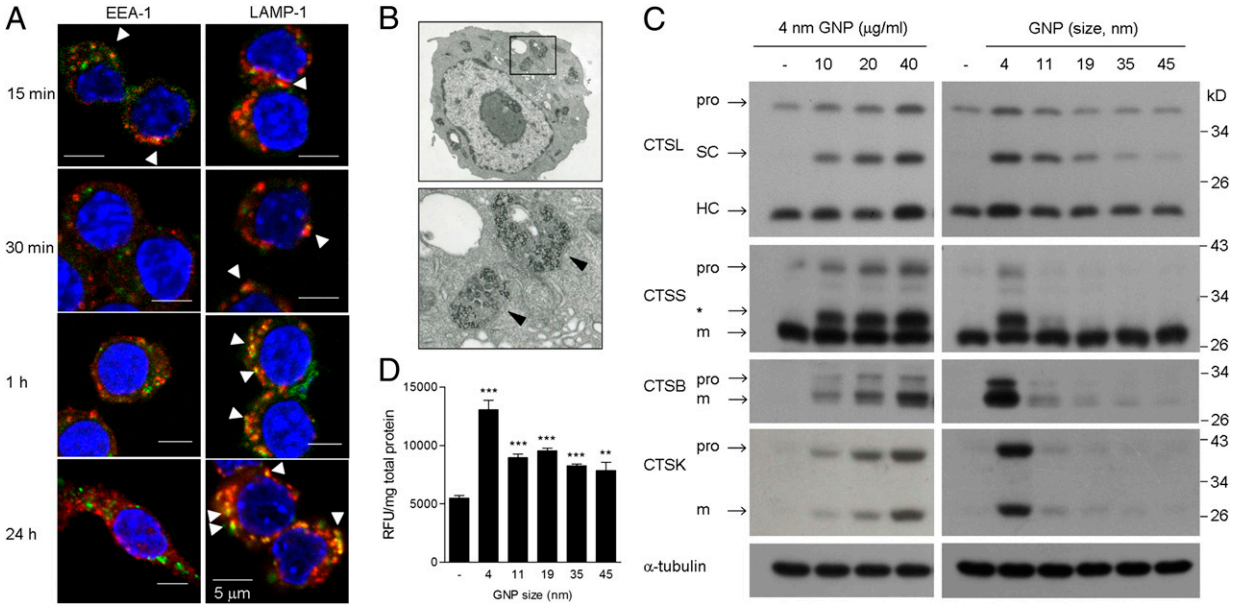

FIGURE 4. GNPs accumulated in lysosomes enhance lysosomal cathepsin expression and activity in Raw264.7 cells. *A*, The intracellular trafficking of GNPs in Raw264.7 cells. Raw264.7 cells were treated with 4-nm F-GNPs at indicated time durations, and their intracellular trafficking was observed with confocal microscopy. The cells were stained with anti-EEA1 Ab (early endosome marker, red), anti–LAMP-1 Ab (late endosome/lysosome marker, red), and Hoechst 33258 (nucleus, blue), respectively. The arrowheads indicate the colocalization of F-GNP and EEA1-positive early endosomes or LAMP-1–positive lysosomes. *B*, Electron microscopy observation of 4-nm GNPs in Raw264.7 cells. Cells were treated with 4-nm GNPs for 24 h and then were fixed and examined by electron microscopy (original magnification ×8000). The image of the *bottom panel* is a higher magnification of the boxed area in the *top panel*. The black arrowheads indicate the locations of GNPs inside macrophages. *C*, The expression of cathepsins in GNP-treated Raw264.7 cells. Raw264.7 cells were incubated with 4-nm GNPs at indicated concentrations (*left panels*) or 40 μg/ml of various sizes of GNPs (*right panels*). The lysates from nontreated and GNP-treated Raw264.7 cells were subjected to immunoblotting using Ab against CTSL, CTSS, CTSB, and CTSK. Pro, m, SC, and HC indicate proform, mature form, single-chain form, and H chain form, respectively. An asterisk (*) indicates that CTSS may have an additional immature form. *D*, Size-dependent GNP enhancement of CTSL enzyme activity. Raw264.7 cells were incubated with various sizes of GNPs at 40 μg/ml for 24 h. The CTSL enzyme activity of lysates from Raw264.7 cells was determined. The CTSL activities of all GNPs were compared with control. The experiments were repeated at least two times.

treated cells. However, no colocalization of TLR9 with CpG-ODNs was observed at the times of 5 and 15 min in GNP-treated cells. To trace further the TLR9 translocation, the phagosomes from GNP-treated Raw264.7 cells were purified and analyzed. The cells were treated with magnetic beads for a short period of time (30–120 min) to allow the phagosomes that contain magnetic beads after uptake to be separated by the magnetic field. We also ruled out the possibility that GNP treatment may affect the phagocytosis ability of Raw264.7 cells (Supplemental Fig. 2*B*). In Fig. 5*B*, we observed that the TLR9 cleavage fragment (c-ter-TLR9, ~65 kDa) was enriched in phagosomes at 120 min after magnetic bead uptake in control macrophages. The translocation of c-ter-TLR9 to phagosomes was inhibited in the GNP-treated Raw264.7 cells at 120 min after phagocytosis of magnetic beads. The lysosomal protein LAMP-1 was used as the indicator of phagosome preparation and was increased after GNP phagocytosis. Upon CpG-ODN stimulation, the TLR9 cleavage and its translocation to phagosomes were increased (38). When we added CpG-ODNs to

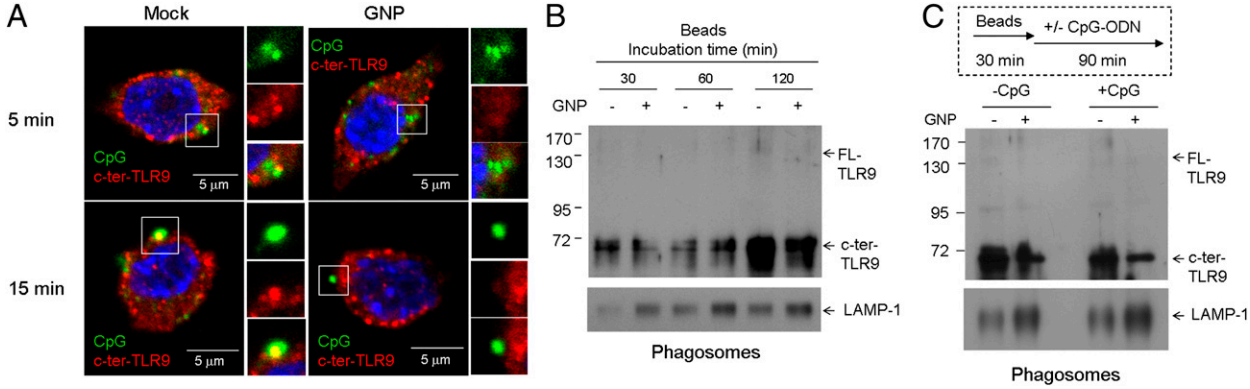

FIGURE 5. GNP impairs TLR9 translocation in response to CpG and TLR9 translocation to phagosomes in Raw264.7 cells. *A*, The translocation of c-ter-TLR9 in response to CpG was inhibited by GNPs. Raw264.7 cells were treated with 40 μg/ml 4-nm GNPs for 24 h and then incubated with CpG-ODN–FITC (3 μM) for 5 and 15 min. Then, cells fixed and stained with anti-TLR9 Ab (red) and Hoechst 33258 (blue) were observed with confocal microscopy. *B* and *C*, The translocation of c-ter-TLR9 to phagosomes was inhibited by GNPs. Raw264.7 cells were treated with magnetic beads and then stimulated without (*B*) or with (*C*) CpG-ODNs (0.5 μM). Magnetic bead-containing phagosomes were purified by magnetic field. The lysates of purified phagosomes from the cells were separated by SDS-PAGE and probed with Abs against the indicated proteins. FL-TLR9, full-length TLR9; c-ter-TLR9, C-terminal fragment of TLR9.

the culture, the translocation of cleaved TLR9 fragments in phagosomes was not altered. Again, the GNP-treated Raw264.7 cells still have a lower level of processed TLR9 in phagosomes than in the control (Fig. 5*C*). Taken together, these data demonstrate that GNPs accumulated in lysosomes could affect the TLR9 translocation in response to CpG-ODNs as well as TLR9 translocation to phagosomes.

GNP binds HMGB-1 in the lysosomes

To explore further the mechanism of GNP-mediated inhibition of the TLR9 signal, the lysosomes were separated from GNP-treated Raw264.7 cells, and GNP-binding proteins in lysosomes were also purified. Fig. 6*A* shows additional proteins that were found in the 4-nm GNP-treated Raw264.7 cells but not in the nontreated cells according to the silver stain of SDS-PAGE. The regions 1–3 mark the proteins that may interact with the GNPs in lysosomes, including molecular mass 55∼72 kDa (region 1), 40∼45 kDa (region 2), and 24∼34 kDa (region 3). The 30 kDa-nucleic acid sensor HMGB-1 has recently been shown to regulate the TLR9-mediated inflammatory responses to CpG-ODNs (6–8). Using anti–HMGB-1 Ab in a Western blot analysis, we can detect HMGB-1 in region 3. The amount of HMGB-1 detected was GNP dose dependent, with more HMGB-1 being found from the 40 μg/ml-treated GNP-binding proteins in lysosomes (Fig. 6*B*). We also detected the single-chain and H chain of CTSL in region 3, but the proform (∼39 kDa) of CTSL was not detected in region 2. The c-ter-TLR9 in region 1 was also found, but no difference was found after GNP treatment. LAMP-1 was used as a nonlysosomal protein contaminant control in the isolated GNP-binding proteins. HMGB-1 is known to be localized in the cytoplasmic space and can be released into the supernatant fraction from cellular organelles during the fractionation procedure (39). To confirm further that GNP can bind with HMGB-1, we prepared the cytoplasmic fraction containing the HMGB-1 protein from Raw264.7 cells as materials for binding to GNP. Western blot analysis revealed that the amount of HMGB-1 in the supernatant decreased as the added GNP increased (Fig. 6*C*, GNP-absorbed panel). Accordingly, increased HMGB-1 was observed with increasing GNP (Fig. 6*C*, GNP-eluted panel). Furthermore, confocal microscopy images show that partial amounts of HMGB-1 were located in LAMP-1–positive lysosomes (Fig. 6*D*), as reported by a previous study (40). These data suggest that GNP-attenuated TLR9 signaling may be through interaction with HMGB-1 in lysosomes.

Discussion

Macrophages are the major professional cells to recognize and respond to nanoparticles in the body (22, 41, 42). Although GNPs are believed to be chemically inert, nonimmunogenic, and biocompatible, our results have shown that TLR9 signaling and function are modulated after internalized GNPs have accumulated in lysosomes. This attenuation of the CpG-ODN–induced TLR9 signaling by GNPs in macrophages is size dependent. The smallest 4-nm size of GNP is the most potent in the inhibition of the TLR9 signal because it contains the highest surface area among the different sizes of GNP. It also reflects the high amount of GNP surface binding to molecules in the lysosomal compartments such as to the common DNA sensor HMGB-1. GNPs, especially at the small size of 4 nm, cannot be considered as cellularly inert because they can modulate the biological function by binding to important signal molecules in cells.

Many nanomaterials have been reported to induce inflammatory responses, such as silica nanoparticles, cetyltrimethylammonium bromide-coated gold nanorod, and titanium dioxide nanoparticles (43–45). However, few studies have focused on the effect of nanoparticles on TLR stimulation. Lucarelli et al. (46) have shown that TLR9 expression was decreased in silica nanoparticle-treated U937 cells. Castillo et al. (47) also showed that tiopronin monolayer-protected silver nanoparticles affected the TLR3 ligand and TLR9 ligand-induced IL-6 secretion in Raw264.7 cells. Bare silver nanoparticles are toxic and need surface modification to achieve low cytotoxicity and high stability (48). In our study, the modulatory effects of GNPs on TLR9-mediated signaling primarily occurred in lysosomes, not the TLR9 mRNA synthesis (Supplemental Fig. 2*A*). Without surface modification, bare GNP showed excellent inhibition of CpG-ODN–induced TLR9 signal-

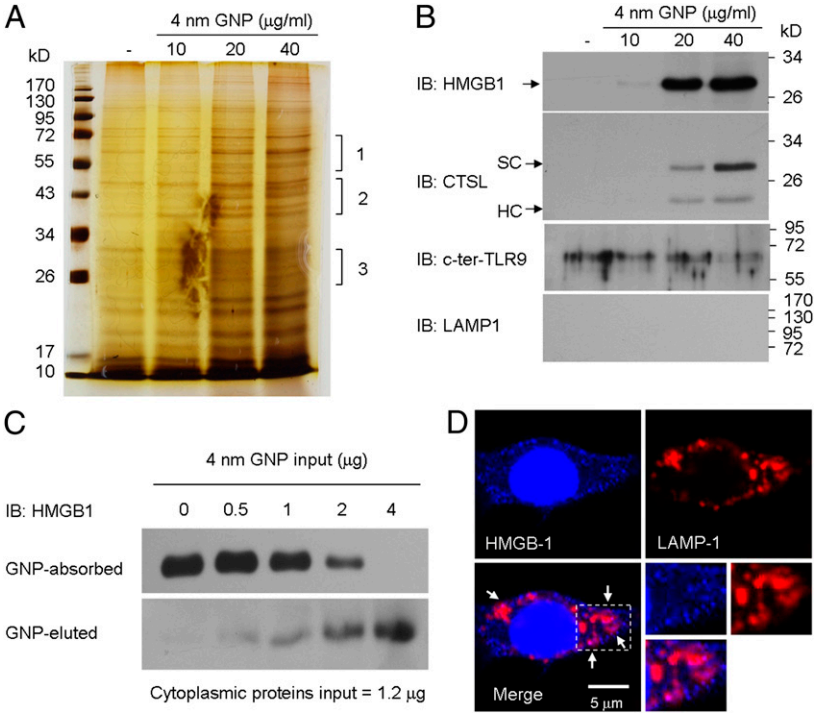

FIGURE 6. GNP binding to HMGB-1 and CTSL in the isolated GNP-containing lysosomes. *A*, Silver staining of purified proteins from GNP-containing lysosomes. Raw264.7 cells were incubated with 4-nm GNPs at indicated concentrations for 24 h. The GNP-containing lysosomes were purified by ultracentrifuge. The lysosomes were lysed, and the GNP-binding proteins were eluted by DTT (see *Materials and Methods*) and run on SDS-PAGE and then silver stained. *B*, The eluted proteins were also separated by SDS-PAGE and probed with Abs against HMGB-1, CTSL, TLR9, and LAMP-1 on Western blot. The LAMP-1 was used as a nonlysosomal protein contaminant control in the isolated GNP-binding proteins. *C*, GNPs bind to HMGB-1. The cytoplasmic proteins containing HMGB-1 were incubated with different amounts of 4-nm GNPs. After centrifugation, the supernatants (GNP-absorbed) and the proteins eluted from GNP-containing pellets by DTT (GNP-eluted) were collected and probed with Ab against HMGB-1. *D*, HMGB-1 was partially located in lysosomes. Raw264.7 cells were fixed and stained with Abs against HMGB-1 and LAMP-1. The arrows indicate that HMGB-1 was colocalized with LAMP-1–positive lysosomes.

ing. This is thus, to our knowledge, the first report of nonconjugated GNPs inhibiting or modulating the TLR9 signaling.

The mechanism for this size-dependent effect is different from other studies. Jiang et al. (24) reported that Herceptin-conjugated GNP could activate the ErbB2 receptor in a size-dependent manner. The Herceptin-conjugated GNPs of 40- or 50-nm size are the most effective to internalize into ErbB2-overexpressed SK-BR-3 cells and therefore more effective with regard to their effect on the conjugated protein. Oh et al. (23) also showed that the cytotoxicity of silica–titania hollow nanoparticles (HNPs) on macrophages was consistent with the cellular internalization efficiency of HNPs. Fifty-nanometer HNPs demonstrated the highest cytotoxicity, and cationic 50-nm HNPs were even more toxic and exhibited the highest uptake efficiency. The findings of these two studies can be explained by the amount of internalization involved. The size of 50 nm is the most efficiently internalized and therefore more effective with regard to its effect on the conjugated protein as well as on surface functioning. In our studies, we used bare nanogold particles that will directly bind to the sulfhydryl or amine residues of molecules in the lysosome, which is the major deposition site after internalization. The 35-nm size of GNP is the most efficiently phagocytosed by professional macrophages (Fig. 2*C*), but the 4-nm GNP is the most potent for modulating the functions in the internalized compartment of lysosomes (Fig. 2*B*). One possibility is that 4-nm GNPs have the largest total surface area compared with other sizes of GNPs (Fig. 2*D*, 2*E*). The large relative surface area of the smaller GNP may increase its binding ability to lysine- or cysteine-rich proteins. Moreover, larger GNP–protein complexes have higher binding avidity (24). In contrast, smaller GNP–protein complexes are unstable, and so GNPs may become more active until they are stabilized by stronger binding, such as with gold–thiol interaction. In addition, proteins interacting with GNPs may experience some blocking of their activities (14, 15). Therefore, the 4-nm GNP size being the most potent for modulating TLR9 functions may be attributable to its large total surface area inside macrophages.

TLR9 elicits the MyD88-dependent pathway involving NIK–IKK–IκB and MAPK pathways (5, 29). In our study, TLR9 signaling was attenuated by GNPs. Therefore, all downstream signaling molecules including IκB/NF-κB, JNK, p38, and ERK should be inhibited as well. However, we found that only IκB/NF-κB and JNK signal pathways could be affected by GNPs (Fig. 3*A*). In addition, the p-p38 and p-ERK pathways were significantly upregulated in GNP-treated macrophages without CpG-ODN stimulation (Fig. 3*B*). These results suggest that the accumulation of GNPs in lysosomes might act as an intracellular stress and further activate MAPK signaling (49). Thus, the inhibition of CpG-ODN–induced p38 and ERK signaling by GNPs could not be observed in our study. However, the activation of MAPK signaling by GNPs may cause the increased expression of TLR9 mRNA (Supplemental Fig. 2*A*) (50). Because we did not find that any cytotoxicity occurred in various sizes of GNPs in macrophages (Fig. 2*A*, *f*), the increased phosphorylation of p38 and ERK, which regulates macrophage survival by inducing the transcription of antiapoptotic genes, may play an important role in the cell proliferation of GNP-treated macrophages.

In studying the mechanisms for how GNPs accumulated in lysosomes impair TLR9 function, we found that GNPs can interact and bind with HMGB-1 in lysosomes (Fig. 6*B*). The nucleic acid sensor HMGB-1 has recently been shown to regulate the TLR9-mediated inflammatory responses to CpG-ODNs (6, 7). HMGB-1 is constitutively associated with TLR9, and its absence impairs the activation of TLR9 in macrophages (6, 8). CpG-ODNs combined with HMGB-1 can enhance the TLR9-mediated TNF-α production (6, 7). Hmgb1$^{-/-}$ macrophages and dendritic cells have reduced recognition of CpG-ODNs (6). In our studies, the GNPs could efficiently bind to HMGB-1. Therefore, we propose that GNP binding to HMGB-1 plays an important role in the attenuation of TLR9 function. The GNP binding to protein can induce conformational change of protein structure (51).The GNP–HMGB-1 complex may change the HMGB-1 conformation and affect the folding or the binding of the HMGB-1–CpG-ODN complex and thus attenuate TLR9 function. Although there are no reports suggesting that the conformational change of the TLR9 dimer that is required for TLR9 activation requires HMGB-1, we also propose that the GNP–HMGB-1 complex might cause impairment of the conformational change of the TLR9 dimer (52). In addition, HMGB-1 accelerates the redistribution of TLR9 to early endosomes in response to CpG-ODNs (6). Therefore, the GNP–HMGB-1 complex may affect the TLR9 redistribution in response to CpG-ODNs (Fig. 5*A*) or phagosomes (Fig. 5*B*, 5*C*). Although we found that GNP binds to HMGB-1, there are other endolysosomal GNP-binding proteins (Fig. 6*A*) that need to be identified and to determine further whether they are involved in the regulation of TLR9 function.

In our study, GNPs can induce expression and activity of CTSL, CTSS, CTSB, and CTSK in a dose- and size-dependent manner (Fig. 4*C*, 4*D*). Specific inhibition of cysteine proteases can block the TLR9 signaling (31, 32). Although there are no confirmatory reports, we presume that the overexpression of cathepsins may increase TLR9 function. However, the elevation of cathepsins by GNPs did not enhance TLR9 function but inhibited it instead. Another explanation for the inhibition of TLR9 function by GNPs is that GNP-induced cathepsin expression and activities may cause TLR9 degradation. Although it blocked excess lysosomal protease activities by a cysteine protease inhibitor, E64d inhibited TNF-α production as expected, but again, it did not restore the GNP-impaired CpG-ODN–induced TNF-α production and also did not recover the GNP-impaired phagosomal translocation of cleaved TLR9 (data not shown). Thus, the mechanism of GNP action is not the same as that of E64d. This suggests that although the TLR9 activation may indeed need protease procession, it also requires other molecules to complete the function; for example, HMGB-1.

Previous studies showed that the inhibition of TLR9 function in macrophages may have beneficial effects in the treatment of some diseases, such as lupus nephritis and autoimmune diseases (53, 54). In this study, we demonstrate that GNPs, especially the small size (4 nm), have a potent modulatory activity in lysosomes once ingested into macrophages. The excellent inhibition of the 4-nm GNP on TLR9 function may offer further possibilities of therapeutic manipulation. Nevertheless, although GNP is not cytotoxic, its signal modulation on TLR9-related or HMGB-1–related functions should be considered when determining safe application to biomedical use.

Acknowledgments

We thank Dr. Chih-Chia Huang for help with TEM and inductively coupled plasma atomic emission spectroscopy examination. We also thank Prof. Kuo-Feng Hua (Institute of Biotechnology, National Ilan University, I-Lan, Taiwan) for kindly providing the RAW-Blue cells.

Disclosures

The authors have no financial conflicts of interest.

References

1. Gordon, S., and P. R. Taylor. 2005. Monocyte and macrophage heterogeneity. *Nat. Rev. Immunol.* 5: 953–964.

2. Akira, S., S. Uematsu, and O. Takeuchi. 2006. Pathogen recognition and innate immunity. *Cell* 124: 783–801.
3. Gordon, S. 2002. Pattern recognition receptors: doubling up for the innate immune response. *Cell* 111: 927–930.
4. Iwasaki, A., and R. Medzhitov. 2010. Regulation of adaptive immunity by the innate immune system. *Science* 327: 291–295.
5. Kumar, H., T. Kawai, and S. Akira. 2009. Pathogen recognition in the innate immune response. *Biochem. J.* 420: 1–16.
6. Ivanov, S., A. M. Dragoi, X. Wang, C. Dallacosta, J. Louten, G. Musco, G. Sitia, G. S. Yap, Y. Wan, C. A. Biron, et al. 2007. A novel role for HMGB1 in TLR9-mediated inflammatory responses to CpG-DNA. *Blood* 110: 1970–1981.
7. Tian, J., A. M. Avalos, S. Y. Mao, B. Chen, K. Senthil, H. Wu, P. Parroche, S. Drabic, D. Golenbock, C. Sirois, et al. 2007. Toll-like receptor 9-dependent activation by DNA-containing immune complexes is mediated by HMGB1 and RAGE. *Nat. Immunol.* 8: 487–496.
8. Yanai, H., T. Ban, Z. Wang, M. K. Choi, T. Kawamura, H. Negishi, M. Nakasato, Y. Lu, S. Hangai, R. Koshiba, et al. 2009. HMGB proteins function as universal sentinels for nucleic-acid-mediated innate immune responses. *Nature* 462: 99–103.
9. Alivisatos, P. 2004. The use of nanocrystals in biological detection. *Nat. Biotechnol.* 22: 47–52.
10. Bhattacharya, R., and P. Mukherjee. 2008. Biological properties of "naked" metal nanoparticles. *Adv. Drug Deliv. Rev.* 60: 1289–1306.
11. Daniel, M. C., and D. Astruc. 2004. Gold nanoparticles: assembly, supramolecular chemistry, quantum-size-related properties, and applications toward biology, catalysis, and nanotechnology. *Chem. Rev.* 104: 293–346.
12. Boisselier, E., and D. Astruc. 2009. Gold nanoparticles in nanomedicine: preparations, imaging, diagnostics, therapies and toxicity. *Chem. Soc. Rev.* 38: 1759–1782.
13. Chen, Y. H., C. Y. Tsai, P. Y. Huang, M. Y. Chang, P. C. Cheng, C. H. Chou, D. H. Chen, C. R. Wang, A. L. Shiau, and C. L. Wu. 2007. Methotrexate conjugated to gold nanoparticles inhibits tumor growth in a syngeneic lung tumor model. *Mol. Pharm.* 4: 713–722.
14. Mukherjee, P., R. Bhattacharya, P. Wang, L. Wang, S. Basu, J. A. Nagy, A. Atala, D. Mukhopadhyay, and S. Soker. 2005. Antiangiogenic properties of gold nanoparticles. *Clin. Cancer Res.* 11: 3530–3534.
15. Tsai, C. Y., A. L. Shiau, S. Y. Chen, Y. H. Chen, P. C. Cheng, M. Y. Chang, D. H. Chen, C. H. Chou, C. R. Wang, and C. L. Wu. 2007. Amelioration of collagen-induced arthritis in rats by nanogold. *Arthritis Rheum.* 56: 544–554.
16. Tsai, C. Y., A. L. Shiau, P. C. Cheng, D. B. Shieh, D. H. Chen, C. H. Chou, C. S. Yeh, and C. L. Wu. 2004. A biological strategy for fabrication of Au/EGFP nanoparticle conjugates retaining bioactivity. *Nano Lett.* 4: 1209–1212.
17. Glazer, E. S., C. Zhu, K. L. Massey, C. S. Thompson, W. D. Kaluarachchi, A. N. Hamir, and S. A. Curley. 2010. Noninvasive radiofrequency field destruction of pancreatic adenocarcinoma xenografts treated with targeted gold nanoparticles. *Clin. Cancer Res.* 16: 5712–5721.
18. Brandenberger, C., B. Rothen-Rutishauser, C. Mühlfeld, O. Schmid, G. A. Ferron, K. L. Maier, P. Gehr, and A. G. Lenz. 2010. Effects and uptake of gold nanoparticles deposited at the air-liquid interface of a human epithelial airway model. *Toxicol. Appl. Pharmacol.* 242: 56–65.
19. Lewinski, N., V. Colvin, and R. Drezek. 2008. Cytotoxicity of nanoparticles. *Small* 4: 26–49.
20. Shukla, R., V. Bansal, M. Chaudhary, A. Basu, R. R. Bhonde, and M. Sastry. 2005. Biocompatibility of gold nanoparticles and their endocytotic fate inside the cellular compartment: a microscopic overview. *Langmuir* 21: 10644–10654.
21. Sadauskas, E., G. Danscher, M. Stoltenberg, U. Vogel, A. Larsen, and H. Wallin. 2009. Protracted elimination of gold nanoparticles from mouse liver. *Nanomedicine* 5: 162–169.
22. Sadauskas, E., H. Wallin, M. Stoltenberg, U. Vogel, P. Doering, A. Larsen, and G. Danscher. 2007. Kupffer cells are central in the removal of nanoparticles from the organism. *Part. Fibre Toxicol.* 4: 10.
23. Oh, W. K., S. Kim, M. Choi, C. Kim, Y. S. Jeong, B. R. Cho, J. S. Hahn, and J. Jang. 2010. Cellular uptake, cytotoxicity, and innate immune response of silica-titania hollow nanoparticles based on size and surface functionality. *ACS Nano* 4: 5301–5313.
24. Jiang, W., B. Y. Kim, J. T. Rutka, and W. C. Chan. 2008. Nanoparticle-mediated cellular response is size-dependent. *Nat. Nanotechnol.* 3: 145–150.
25. Mottram, P. L., D. Leong, B. Crimeen-Irwin, S. Gloster, S. D. Xiang, J. Meanger, R. Ghildyal, N. Vardaxis, and M. Plebanski. 2007. Type 1 and 2 immunity following vaccination is influenced by nanoparticle size: formulation of a model vaccine for respiratory syncytial virus. *Mol. Pharm.* 4: 73–84.
26. Chao, L. K., P. C. Liao, C. L. Ho, E. I. Wang, C. C. Chuang, H. W. Chiu, L. B. Hung, and K. F. Hua. 2010. Anti-inflammatory bioactivities of honokiol through inhibition of protein kinase C, mitogen-activated protein kinase, and the NF-kappaB pathway to reduce LPS-induced TNFalpha and NO expression. *J. Agric. Food Chem.* 58: 3472–3478.
27. Frens, G. 1973. Controlled nucleation for the regulation of the particle size in monodisperse gold suspensions. *Nature* 241: 20–22.
28. Edwards, A. D., S. S. Diebold, E. M. Slack, H. Tomizawa, H. Hemmi, T. Kaisho, S. Akira, and C. Reis e Sousa. 2003. Toll-like receptor expression in murine DC subsets: lack of TLR7 expression by CD8 alpha+ DC correlates with unresponsiveness to imidazoquinolines. *Eur. J. Immunol.* 33: 827–833.
29. Takeshita, F., I. Gursel, K. J. Ishii, K. Suzuki, M. Gursel, and D. M. Klinman. 2004. Signal transduction pathways mediated by the interaction of CpG DNA with Toll-like receptor 9. *Semin. Immunol.* 16: 17–22.
30. Kawai, T., and S. Akira. 2007. TLR signaling. *Semin. Immunol.* 19: 24–32.
31. Matsumoto, F., S. Saitoh, R. Fukui, T. Kobayashi, N. Tanimura, K. Konno, Y. Kusumoto, S. Akashi-Takamura, and K. Miyake. 2008. Cathepsins are required for Toll-like receptor 9 responses. *Biochem. Biophys. Res. Commun.* 367: 693–699.
32. Park, B., M. M. Brinkmann, E. Spooner, C. C. Lee, Y. M. Kim, and H. L. Ploegh. 2008. Proteolytic cleavage in an endolysosomal compartment is required for activation of Toll-like receptor 9. *Nat. Immunol.* 9: 1407–1414.
33. Chircorian, A., and A. M. Barrios. 2004. Inhibition of lysosomal cysteine proteases by chrysotherapeutic compounds: a possible mechanism for the antiarthritic activity of Au(I). *Bioorg. Med. Chem. Lett.* 14: 5113–5116.
34. Weidauer, E., Y. Yasuda, B. K. Biswal, M. Cherny, M. N. James, and D. Brömme. 2007. Effects of disease-modifying anti-rheumatic drugs (DMARDs) on the activities of rheumatoid arthritis-associated cathepsins K and S. *Biol. Chem.* 388: 331–336.
35. Latz, E., A. Schoenemeyer, A. Visintin, K. A. Fitzgerald, B. G. Monks, C. F. Knetter, E. Lien, N. J. Nilsen, T. Espevik, and D. T. Golenbock. 2004. TLR9 signals after translocating from the ER to CpG DNA in the lysosome. *Nat. Immunol.* 5: 190–198.
36. Chockalingam, A., J. C. Brooks, J. L. Cameron, L. K. Blum, and C. A. Leifer. 2009. TLR9 traffics through the Golgi complex to localize to endolysosomes and respond to CpG DNA. *Immunol. Cell Biol.* 87: 209–217.
37. Ewald, S. E., B. L. Lee, L. Lau, K. E. Wickliffe, G. P. Shi, H. A. Chapman, and G. M. Barton. 2008. The ectodomain of Toll-like receptor 9 is cleaved to generate a functional receptor. *Nature* 456: 658–662.
38. Sepulveda, F. E., S. Maschalidi, R. Colisson, L. Heslop, C. Ghirelli, E. Sakka, A. M. Lennon-Duménil, S. Amigorena, L. Cabanie, and B. Manoury. 2009. Critical role for asparagine endopeptidase in endocytic Toll-like receptor signaling in dendritic cells. *Immunity* 31: 737–748.
39. Merenmies, J., R. Pihlaskari, J. Laitinen, J. Wartiovaara, and H. Rauvala. 1991. 30-kDa heparin-binding protein of brain (amphoterin) involved in neurite outgrowth. Amino acid sequence and localization in the filopodia of the advancing plasma membrane. *J. Biol. Chem.* 266: 16722–16729.
40. Lee, H., N. Shin, M. Song, U. B. Kang, J. Yeom, C. Lee, Y. H. Ahn, J. S. Yoo, Y. K. Paik, and H. Kim. 2010. Analysis of nuclear high mobility group box 1 (HMGB1)-binding proteins in colon cancer cells: clustering with proteins involved in secretion and extranuclear function. *J. Proteome Res.* 9: 4661–4670.
41. Cho, W. S., M. Cho, J. Jeong, M. Choi, B. S. Han, H. S. Shin, J. Hong, B. H. Chung, J. Jeong, and M. H. Cho. 2010. Size-dependent tissue kinetics of PEG-coated gold nanoparticles. *Toxicol. Appl. Pharmacol.* 245: 116–123.
42. Simberg, D., J. H. Park, P. P. Karmali, W. M. Zhang, S. Merkulov, K. McCrae, S. N. Bhatia, M. Sailor, and E. Ruoslahti. 2009. Differential proteomics analysis of the surface heterogeneity of dextran iron oxide nanoparticles and the implications for their in vivo clearance. *Biomaterials* 30: 3926–3933.
43. Choi, J., Q. Zheng, H. E. Katz, and T. R. Guilarte. 2010. Silica-based nanoparticle uptake and cellular response by primary microglia. *Environ. Health Perspect.* 118: 589–595.
44. Bartneck, M., H. A. Keul, S. Singh, K. Czaja, J. Bornemann, M. Bockstaller, M. Moeller, G. Zwadlo-Klarwasser, and J. Groll. 2010. Rapid uptake of gold nanorods by primary human blood phagocytes and immunomodulatory effects of surface chemistry. *ACS Nano* 4: 3073–3086.
45. Morishige, T., Y. Yoshioka, A. Tanabe, X. Yao, S. Tsunoda, Y. Tsutsumi, Y. Mukai, N. Okada, and S. Nakagawa. 2010. Titanium dioxide induces different levels of IL-1beta production dependent on its particle characteristics through caspase-1 activation mediated by reactive oxygen species and cathepsin B. *Biochem. Biophys. Res. Commun.* 392: 160–165.
46. Lucarelli, M., A. M. Gatti, G. Savarino, P. Quattroni, L. Martinelli, E. Monari, and D. Boraschi. 2004. Innate defence functions of macrophages can be biased by nano-sized ceramic and metallic particles. *Eur. Cytokine Netw.* 15: 339–346.
47. Castillo, P. M., J. L. Herrera, R. Fernandez-Montesinos, C. Caro, A. P. Zaderenko, J. A. Mejías, and D. Pozo. 2008. Tiopronin monolayer-protected silver nanoparticles modulate IL-6 secretion mediated by Toll-like receptor ligands. *Nanomedicine (Lond)* 3: 627–635.
48. Johnston, H. J., G. Hutchison, F. M. Christensen, S. Peters, S. Hankin, and V. Stone. 2010. A review of the in vivo and in vitro toxicity of silver and gold particulates: particle attributes and biological mechanisms responsible for the observed toxicity. *Crit. Rev. Toxicol.* 40: 328–346.
49. Roux, P. P., and J. Blenis. 2004. ERK and p38 MAPK-activated protein kinases: a family of protein kinases with diverse biological functions. *Microbiol. Mol. Biol. Rev.* 68: 320–344.
50. Chang, J. H., J. Y. Park, and S. K. Kim. 2006. Dependence on p38 MAPK signalling in the up-regulation of TLR2, TLR4 and TLR9 gene expression in Trichomonas vaginalis-treated HeLa cells. *Immunology* 118: 164–170.
51. Jiang, X., J. Jiang, Y. Jin, E. Wang, and S. Dong. 2005. Effect of colloidal gold size on the conformational changes of adsorbed cytochrome c: probing by circular dichroism, UV-visible, and infrared spectroscopy. *Biomacromolecules* 6: 46–53.
52. Latz, E., A. Verma, A. Visintin, M. Gong, C. M. Sirois, D. C. Klein, B. G. Monks, C. J. McKnight, M. S. Lamphier, W. P. Duprex, et al. 2007. Ligand-induced conformational changes allosterically activate Toll-like receptor 9. *Nat. Immunol.* 8: 772–779.
53. Anders, H. J., V. Vielhauer, V. Eis, Y. Linde, M. Kretzler, G. Perez de Lema, F. Strutz, S. Bauer, M. Rutz, H. Wagner, et al. 2004. Activation of toll-like receptor-9 induces progression of renal disease in MRL-Fas(lpr) mice. *FASEB J.* 18: 534–536.
54. Hennessy, E. J., A. E. Parker, and L. A. O'Neill. 2010. Targeting Toll-like receptors: emerging therapeutics? *Nat. Rev. Drug Discov.* 9: 293–307.